Supporting Information

Synthesis, X-ray structure, physicochemical properties and anticancer activity of *mer* and *fac* Ru(III) triphenylphosphine complexes with a benzothiazole derivative as a co-ligand

Monika Richert[*1], *Mariusz Walczyk*[2], *Marcin Janusz Cieślak*[3], *Julia Kaźmierczak-Barańska*[3], *Karolina Królewska-Golińska*[3], *Grzegorz Wrzeszcz*[2], *Tadeusz M. Muzioł*[2], *Stanisław Biniak*[2]

[1]Faculty of Pharmacy, Collegium Medicum in Bydgoszcz, Nicolaus Copernicus University in Toruń; Jurasza 2; 85-094 Bydgoszcz, Poland;

E-mail: monika.richert@cm.umk.pl, phone: +48 52 585-38-03, Fax: +48 52 585-38-04

[2]Faculty of Chemistry, Nicolaus Copernicus University in Toruń; Gagarina 7, 87-100 Toruń, Poland

[3]Centre of Molecular and Macromolecular Studies, Polish Academy of Sciences, Sienkiewicza 112, 90-363 Lódź, Poland

Corresponding Authors

*E-mail: monika.richert@cm.umk.pl

*E-mail: marcin@cbmm.lodz.pl – biological part

Table of content

	Page
Elemental analysis of dmpbt	S3
Figure S1. IR spectrum of dmpbt	S3
Figure S2. ^{1}H NMR spectrum of dmpbt in DMSO	S3
Table S1. Crystal data and structure refinement for (**2**) and (**2'**)	S4
Table S2. IR spectral data of complexes *mer*-Ru(III) (1) and *fac*-Ru(III) (2) and ligands: dmpbt, PPh_3	S5
Figure S3. X-band (9.3300 GHz) EPR spectrum of powdered *mer*-[$RuCl_3(PPh_3)$(dmpbt)] (**1**) at room temperature	S6
X-ray description of (**2'**) and its comparison with (**2**)	S6
Figure S4. Mutual ring orientations in (**2**) (left) and (**2'**) (right) clearly show clockwise rotation of phenyl rings along Ru-P bond	S9
Table S3. Selected bonds lengths (Å) for (**2**) and (**2'**)	S10
Figure S5. The survival rate of HeLa cells after 48 hours of incubation with compound (**1**), (**2**) (dmpbt), and *cis*-Pt	S10
Figure S6. The survival rate of K562 cells after 48 hours of incubation with compound (**1**), (**2**), (dmpbt), *cis*-Pt	S11
Figure S7. The survival rate of A549 cells after 48 hours of incubation with compound (**1**), (dmpbt) and *cis*-Pt	S11
Figure S8. The survival rate of HUVEC cells after 48 hours of incubation with compound (**1**), (**2**), (dmpbt), and *cis*-Pt	S12
Figure S9. The survival rate of A549 cells after 48 hours of incubation with compound (**1**), and *cis*-Pt	S12
Figure S10. The survival rate of HUVEC cells after 48 hours of incubation with compound (**1**), (**2**), and *cis*-Pt	S13
Digestion of plasmid DNA with BamHI restriction nuclease (experimental and results description)	S13
Figure S11. The influence of test compounds, *cis*-Pt and daunorubicin on digestion of plasmid DNA with endonuclease *BamH1*. M – DNA marker; lane 1 – non-digested plasmid DNA; lane 2 – plasmid DNA treated with *BamH1* (linearized plasmid DNA); 3 – plasmid DNA + Daunorubicin (100 μM); lane 4 – plasmid DNA + Daunorubicin (10 μM); lane 5 - plasmid DNA + (**1**) (100 μM); lane 6 – plasmid DNA + (**1**) (10 μM); lane 7 – plasmid DNA + (**2**) (100 μM); lane 8 – plasmid DNA + (**2**) (10 μM); lane 9 – plasmid DNA + (dmpbt) (100 μM); lane 10 – plasmid DNA + (dmpbt) (10 μM); lane 11 – plasmid DNA+ *cis*-Pt (100 μM); lane 12 – plasmid DNA + *cis*-Pt (10 μM). Samples in lanes 3-12 were digested with *BamH1*.	S15
Interaction of (**1**), (**2**), (dmpbt), and *cis*-Pt with DNA – circular dichroism (CD) (experimental and results description)	S15
Figure S12. CD spectra of calf thymus DNA recorded in the presence of compounds (**1**), (dmpbt), (**2**), *cis*-Pt and daunorubicin. Spectra were recorded at room temperature, 15 min. after addition of test compounds (50 μM). DNA + 0.5% DMSO served as a control.	S16

Dmpbt ligand was characterized by elemental analysis, IR (**Figure S1**) and ^{1}H NMR data (**Figure S2**).

Elemental analysis for $C_{12}H_{11}N_3S$. Calculated (%): C, 62.86; H, 4.84; N, 18.33. Found (%): C, 62.84; H, 4.82; N, 18.36%.

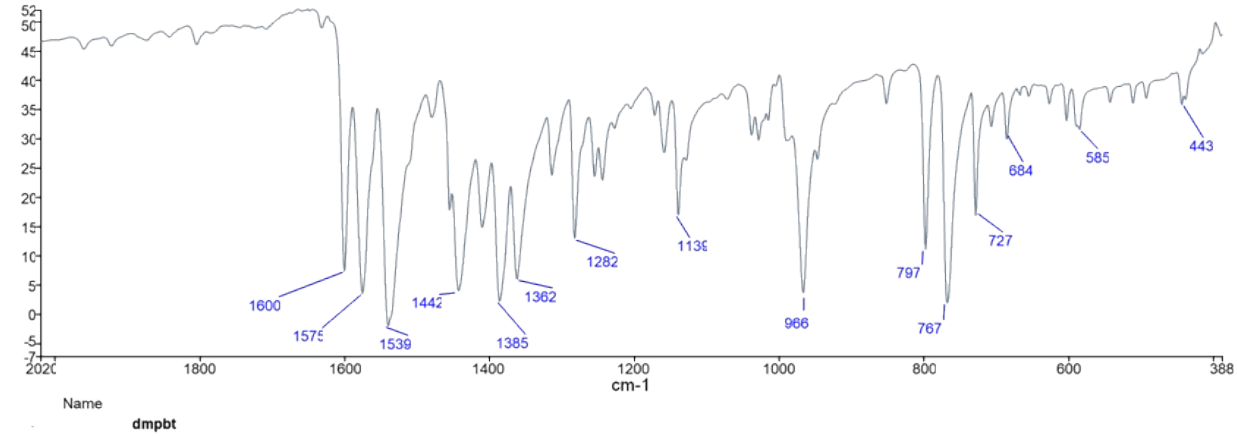

Figure S1. IR spectrum of dmpbt

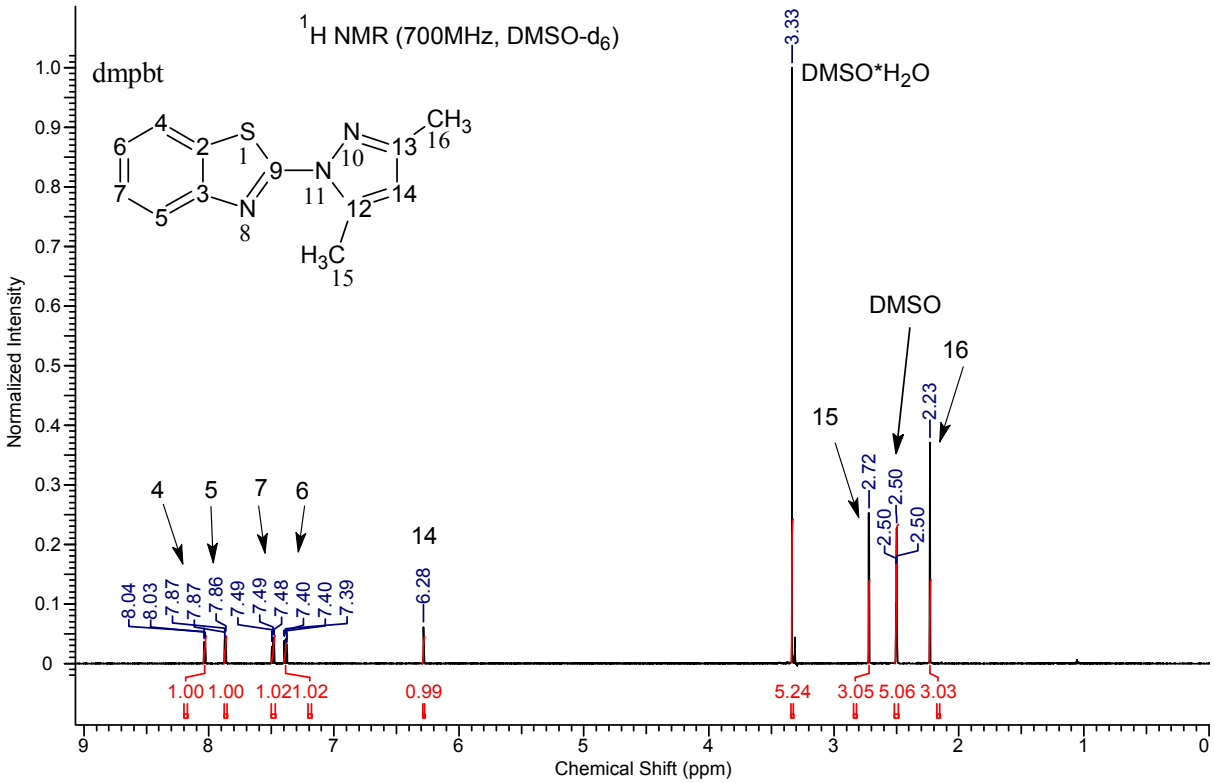

Figure S2. ^{1}H NMR spectrum of dmpbt in DMSO

^{1}H NMR (700 MHz, DMSO-d_6), δ ppm 2.23 (s, 3 H), 2.72 (s, 3 H), 6.28 (s, 1 H), 7.32 - 7.41 (m, 1 H) 7.48 (m, 1 H) 7.82 - 7.89 (m, 1 H) 7.99 - 8.07 (m, 1 H)

Table S1. Crystal data and structure refinement for (**2**) and (**2'**)

Parameters	**(2)**	**(2')**
Empirical formula	$C_{30}H_{28}Cl_3N_3PRuS$	$C_{32}H_{32}Cl_3N_3OPRuS$
Formula weight	717.00	745.05
Temperature [K]	293(2)	293(2)
Wavelength [Å]	0.71073	0.71073
Crystal system, space group	Triclinic, P –1	Triclinic, P –1
Unit cell dimensions [Å] and [°]	a = 8.5500(9) b = 10.1649(11) c = 17.926(2) α = 92.169(10) β = 97.822(10) γ = 99.235(9)	a = 10.0260(10) b = 11.6073(13) c = 15.3369(12) α = 80.329(8) β = 88.746(7) γ = 65.886(10)
Volume [$Å^3$]	1520.6(3)	1603.8(3)
Z, Calculated density [mg/m^3]	2, 1.566	2, 1.543
Absorption coefficient [mm^{-1}]	0.930	0.885
F(000)	726	758
Crystal size [mm]	0.34 x 0.07 x 0.04	0.44 x 0.32 x 0.15
Theta range for data collection [°]	2.03 to 25.02	2.171 to 26.372
Limiting indices	-9 ≤ h ≤ 10 -12 ≤ k ≤ 11	-12<=h<=12 -14<=k<=14
Reflections collected / unique	8868 / 5358 [R(int) = 0.1162]	10423 / 6558 [R(int) = 0.0573]
Completeness to theta	25.02 97.3 %	25.242° 99.9 %
Absorption correction	Numerical	Numerical
Max. and min. transmission	0.9639 and 0.7434	0.879 and 0.697
Refinement method	Full-matrix least-squares on F^2	Full-matrix least-squares on F^2
Data/restraints/parameters	5358 / 12 / 372	6558 / 20 / 391
Goodness-of-fit on F^2	0.972	1.037
Final R indices [I>2sigma(I)]	R1[a] = 0.0844, wR2[b] = 0.1943	R1[a] = 0.0411, wR2[b] = 0.0948
R indices (all data)	R1[a] = 0.1810, wR2[b] = 0.2425	R1[a] = 0.0589, wR2[b] = 0.1079
Extinction coefficient	----	----
Largest diff. peak and hole [$e.Å^{-3}$]	1.842 and -0.756	0.653 and -0.724

[a] $R1 = \Sigma ||F_0| - |F_c|| / \Sigma |F_0|$

[b] $wR2 = [\Sigma w(F_0^2 - F_c^2)^2 / \Sigma (w(F_0^2)^2)]^{1/2}$

Table S2. IR spectral data of complexes *mer*-Ru(III) (**1**) and *fac*-Ru(III) (**2**) and ligands: dmpbt, PPh_3

ν(C=N) (pyr) 1579, ν(C=N) (btz) 1512, ν(Ru-P) 442, ν(Ru-N) 420, 407, 391, 364 ν(Ru-Cl) 329, 291, 245, 193, 142 cm^{-1}

Modes	Wavenumbers (cm^{-1})			
	***mer*-Ru(1)**	***fac*-Ru(2)**	**dmpbt[1]**	**PPh_3[2]**
ν(C=N) (pyr)	1579	1583	1602	
ν(C=N) (btz)	1512	1508	1536	
ν(N-N)	1061 1157 1188	1061 1159 1188	1026 1139 1158	
ν(P-C)	1432 1089 741 695 519	1435 1091 749 699 525		420_s 499_{as}
ν(Ru-P)	442	448 439		
ν(Ru-N)	420 407 391 364	414 407 391 369		
ν(Ru-Cl)	329 291 245 193 142	329 291 247 194 143		
ν(O-H)	-	3451		

(pyr-pyrazole, btz- benzothiazole)

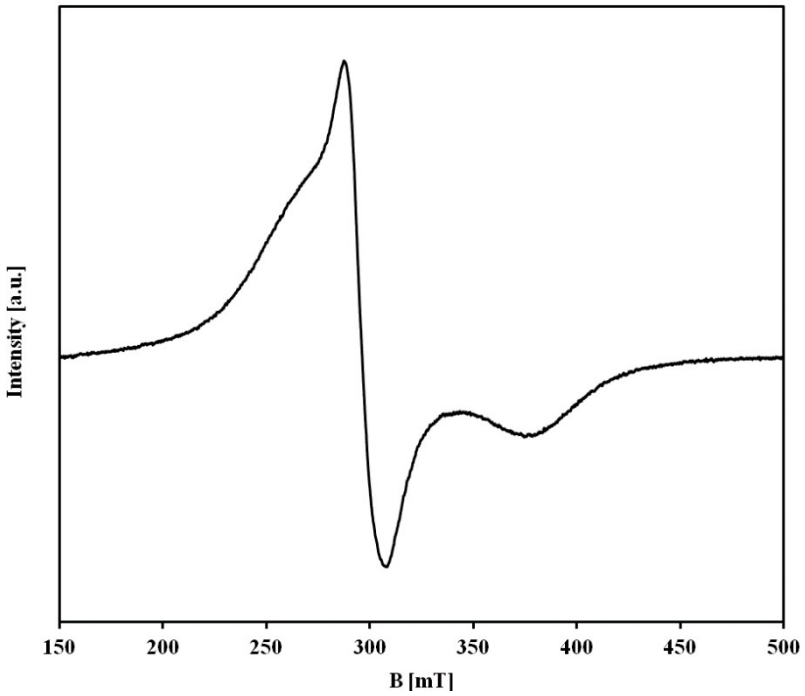

Figure S3. X-band (9.3300 GHz) EPR spectrum of powdered *mer*-[$RuCl_3(PPh_3)$(dmpbt)] (**1**) at room temperature.

X-ray description of (2') and its comparison with (2)

The *fac*-[$RuCl_3(PPh_3)$(dmpbt)]·EtOH (**2'**) crystallized also in the triclinic P-1 space group with all atoms in general positions and the whole molecule given by the formulae in the asymmetric unit. For (**2'**) a positional disorder is observed for hydroxyl group of ethanol molecule and for the minor (0.17) position hydrogen atom attached to this group is also missing. In (**2'**) the ruthenium coordination sphere also adopts slightly distorted octahedral environment and its content is the same as in *fac*-[$RuCl_3(PPh_3)$(dmpbt)]·H_2O (**2**). The main difference concerns Cl3 chloride ions which form slightly shorter bond in (**2'**) (2.3048(10) vs. 2.326(3) Å, in (**2'** and **2**, respectively). In (**2'**) distances in the coordination sphere fall into two ranges: shorter bonds were found for nitrogen atoms [2.098(3) and 2.113(3) Å] and longer for phosphorous [2.3649(9) Å] and chlorine atoms [from 2.3048(10) to 2.4442(10) Å]. Their position according to P1, N14 and N1 atoms is the same as in (**2**). Angles between these *trans* positioned atoms range from 171.27(7) to 178.84(3)º. *cis* positioned atoms form angles

ranging from 77.36(10) to 98.37(7)º. The smallest value is observed for the chelate ring. The benzothiazole ligand is flat within rms deviation of 0.095 Å and even the chelate ring remains flat within rms deviation of 0.055 Å. C2 and six –membered rings form the smallest dihedral angle of 1.85º. The whole ligand remains planar and the biggest angle between its rings is 13.29º for N10 and S8 rings. Three phenyl rings from triphenylphosphine are planar within 0.012 Å. They are twisted and the angles between them are 54.37, 68.76 and 87.44º for C21/C41, C21/C31 and C31/C41 phenyl rings, respectively. The smallest value is found for C21 and C41 phenyl ring as it was also for (**2**), but in this case C31 and C41 rings instead of C21 and C31 ones are perpendicularly oriented. Mutual orientation of the phenyl rings results from intramolecular C-H…Cl hydrogen bonds and steric hindrance as well as numerous intramolecular interactions formed between aromatic rings, mainly involving C41 phenyl group. Comparison of (**2**) and (**2'**) reveal only minor differences in Ru-X bond lengths and valence angles of the coordination sphere. The dihedral angles formed between benzothiazole molecule and phenyl rings are also similar being 29.41 (C21), 67.47 (C31), 26.73° (C41) in (**2**) and 23.61 (C21), 60.86 (C31), 39.93° (C41) in (**2'**). The most important differences can be observed between torsion angles around Ru-P bond (Table ILE Sup).There are four bonds formed in the basal plane of ruthenium (Ru-N1, N14, Cll2, Cl3) and three created by phosphorous (P-C21, C31, C41). Hence, in Newman projection not all atoms can be maximally separated and adopt 60°. It can be seen that angles are similar for N1(**2**) and N14(**2'**) as well as Cl2(**2**) and Cl3(**2'**). In (**2'**) N14-Ru1-P1-C21 torsion angle is -0.50°, whereas N1-Ru1-P1-C41 is 43.02°. In (**2**) these angles are -44.90 and -0.71°, respectively. It indicates that in (**2'**) N14 and C21 are in the closest proximity (eclipsed conformation) and hence N14 and C21 rings are superposed forming intramolecular stacking interactions. However, in (**2**) such contacts were found for N1 and C41 rings. Hence, looking along P-Ru

(P in front of the figure) orientation of triphenylphosphine is rotated by approximately 44° clockwise going from (**2**) to (**2'**).

The unit cell is slightly bigger for **2'** what can be easily explained by presence of ethanol instead of water molecule in the crystal lattice. EtOH molecule is involved in hydrogen bond network *via* its major population O51-H51 hydroxyl group and Cl1[x, y, z] chlorine ion. In general, chlorides form several intramolecular hydrogen bonds with C3-H3, C16-H16 and C32-H32 groups. Additionally, there is intermolecular C42-H42…N1 ring interaction which also affects the configuration of the complex molecule and numerous π-π interactions between slightly inclined rings of benzothiazole ligands and phenyl rings of triphenylphosphine. In the network the closest Ru-Ru distances are 8.523 and 8.496 Å and, hence in the packing we observe pattern similar to **2** but with *ac* layers composed of zigzags running along c axis. Two molecules related by [-x, 1-y, -z] operator form most of intermolecular interactions in the cell mainly via π-π stacking interactions between benzothiazole rings. Subsequently, there is edge-to-face π-π interaction between N10 and C31[-x, 1-y, 1-z] rings, C16-H16B…C31[-x, 1-y, 1-z] ring interactions and C23-H23…Cl3[-x, 1-y, 1-z] hydrogen bond. Surprisingly, two ruthenium(III) ions separated by long distance of 11.849 Å are coupled by quite strong interactions, namely π-π interactions between phenyl rings of the triphenylphosphine prevail but contact between C35-H35 bond and C41[1-x,-y, 1-z] ring was also detected.

Both structures, **2** and **2'**, show similar packing patterns of rather loosely arranged complex moieties with Ru-Ru distance 8.058 and 8.706 vs. 8.496 and 8.523 Å in zigzag and 8.550 vs. 9.803 Å between zigzags, respectively. There are some similarities: both structures can be described as forming zigzags with the strongest interactions created by molecules oriented head-to-head with benzothiazole ligands forming stacking interactions, in both structures prevail π-π interactions. These molecules seem to form much stronger interactions than any

other. To find differences we analyzed intermolecular interactions formed by phenyl rings of triphenylphosphine susceptible to rotation. We found that in **2'** there are six π-π interactions mainly between differently oriented phenyl rings. These contacts are lost after rotation or even steric hindrance and short distances may occur. Similarly, there are C16-H16B…C31[-x, 1-y, 1-z] phenyl ring and C23-H23…Cl3[-x, 1-y, 1-z] hydrogen bond which seem to be also lost due to rotation by 45°. In **2** there are solely seven π-π interactions which are mostly lost due to rotation and sometimes inacceptable short contacts may occur.

Summarizing, we found that subtle differences in formed interactions occurred. Rotation resulted in breaking of interactions and formation of unreasonably short contacts. Hence, the original lattice cannot be maintained and significant changes must occur. In the reported structures of **2** and **2'** rotation of phenyl rings of triphenylphosphine is a driving force of these changes. Additionally, despite solvent molecules are not involved in robust network of interactions and seem to be an auxiliary factor, they affect heavily packing and eventually the formed lattice. The separation between Ru(III) ions is significant and different interaction pathway might affect magnetic properties.

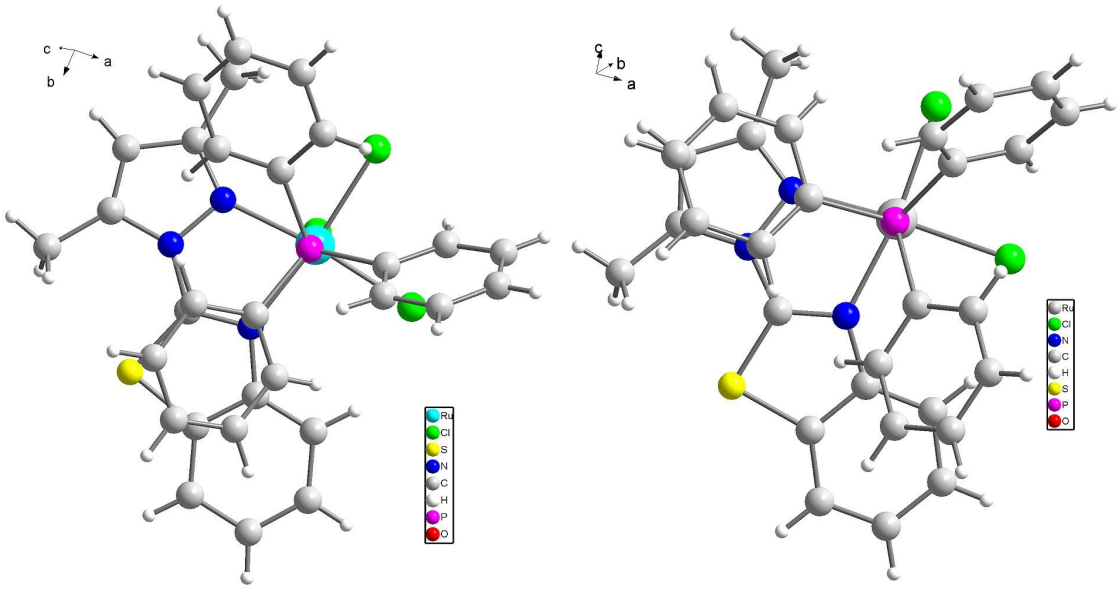

Figure S4. Mutual ring orientations in (**2**) (left) and (**2'**) (right) clearly show clockwise rotation of phenyl rings along Ru-P bond.

Table S3. Selected bonds lengths (Å) for (**2**) and (**2'**)

Complex	**(2)**		**(2')**	
Distances [Å]				
	Ru1-N14	2.083(9)	Ru1-N14	2.098(3)
	Ru1-N1	2.118(8)	Ru1-N1	2.113(3)
	Ru1-Cl3	2.326(3)	Ru1-Cl3	2.3048(10)
	Ru1-Cl2	2.326(3)	Ru1-Cl2	2.3219(9)
	Ru1-P1	2.374(4)	Ru1-P1	2.3649(10)
	Ru1-Cl1	2.438(4)	Ru1-Cl1	2.4442(10)
Angles [°]				
	N14-Ru1-N1	77.5(4)	N14-Ru1-N1	77.36(10)
	N14-Ru1-Cl2	172.3(3)	N14-Ru1-Cl3	94.04(8)
	N1-Ru1-Cl2	95.6(2)	N1-Ru1-Cl3	171.27(7)
	N14-Ru1-Cl3	96.5(3)	N14-Ru1-Cl2	174.74(8)
	N1-Ru1-Cl3	173.9(2)	N1-Ru1-Cl2	98.37(7)
	Cl2-Ru1-Cl3	90.39(12)	Cl3-Ru1-Cl2	90.13(4)
	N14-Ru1-P1	91.3(3)	N14-Ru1-P1	94.11(8)
	N1-Ru1-P1	93.1(3)	N1-Ru1-P1	91.97(7)
	Cl2-Ru1-P1	92.60(13)	Cl3-Ru1-P1	90.19(4)
	Cl3-Ru1-P1	86.09(12)	Cl2-Ru1-P1	89.07(3)
	N14-Ru1-Cl1	85.3(3)	N14-Ru1-Cl1	86.43(8)
	N1-Ru1-Cl1	89.1(3)	N1-Ru1-Cl1	87.15(7)
	Cl2-Ru1-Cl1	91.06(13)	Cl3-Ru1-Cl1	90.79(4)
	Cl3-Ru1-Cl1	91.30(12)	Cl2-Ru1-Cl1	90.31(4)
	P1-Ru1-Cl1	175.51(13)	P1-Ru1-Cl1	178.84(3)

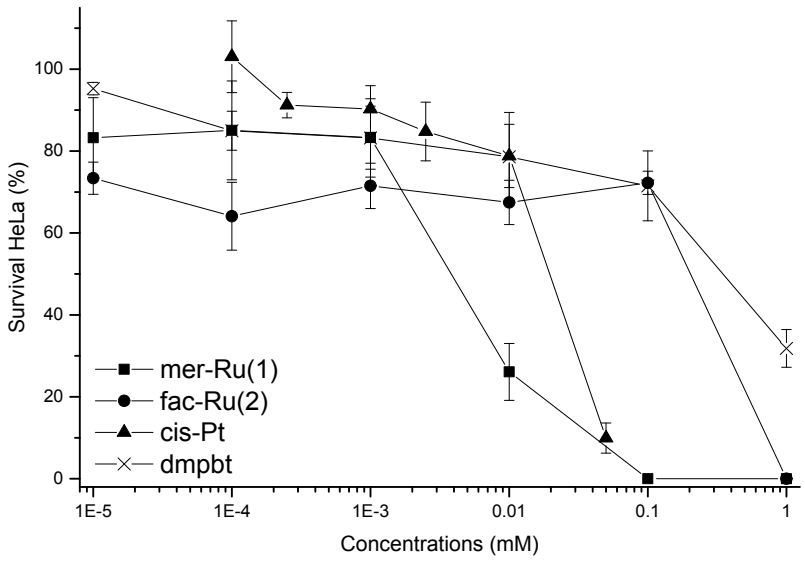

Figure S5. The survival rate of HeLa cells after 48 hours of incubation with compound (**1**), (**2**) (dmpbt), and *cis*-Pt.

* compound (**2**) precipitated at a concentration of 1 mM in the cell culture (the results were discarded)

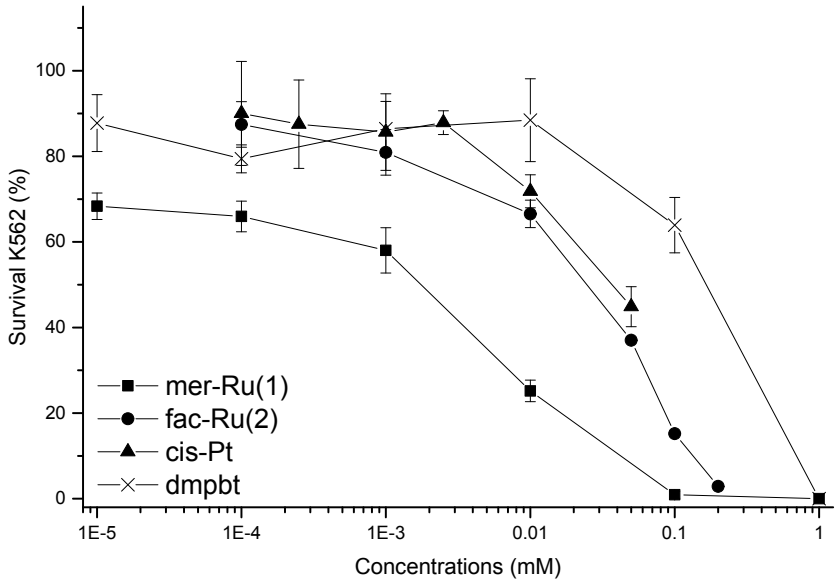

Figure S6. The survival rate of K562 cells after 48 hours of incubation with compound (**1**), (**2**), (dmpbt), *cis*-Pt.

* compound (**2**) precipitated at a concentration of 1 mM in the cell culture (the results were discarded)

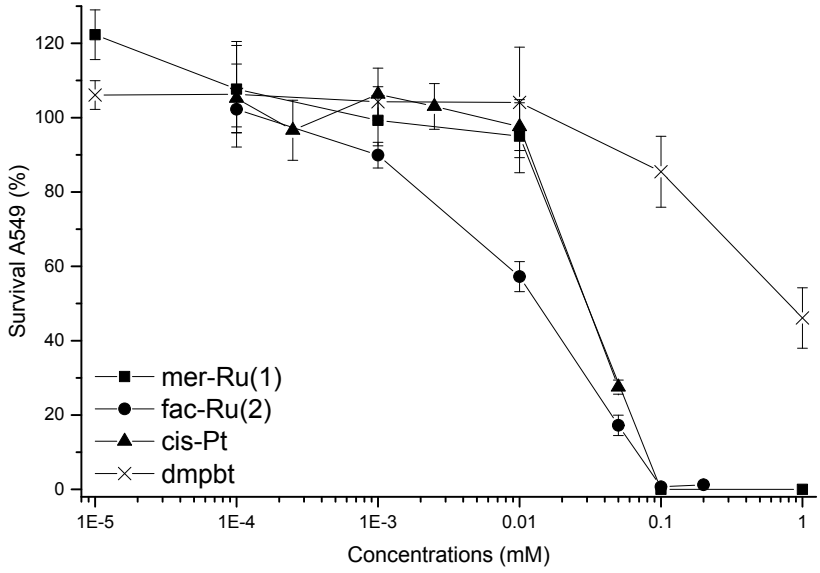

Figure S7. The survival rate of A549 cells after 48 hours of incubation with compound (**1**), (dmpbt) and *cis*-Pt.

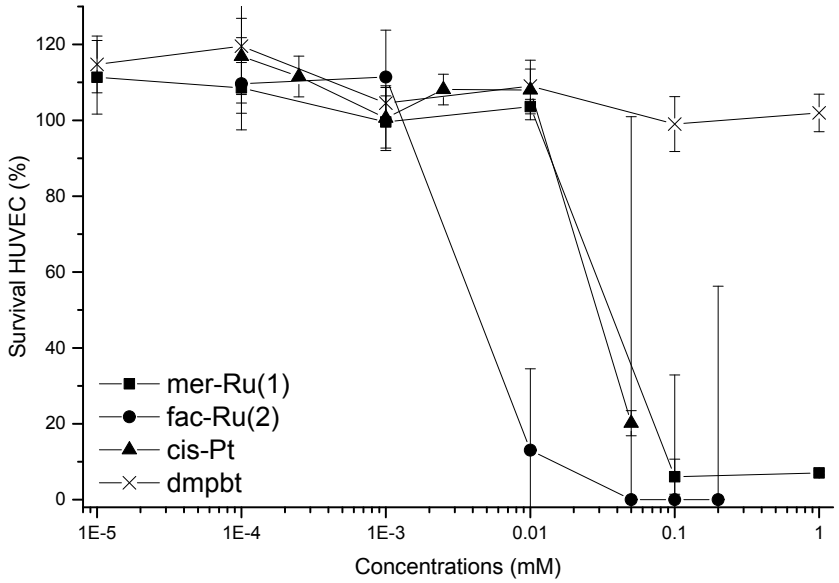

Figure S8. The survival rate of HUVEC cells after 48 hours of incubation with compound (**1**), (**2**), (dmpbt), and *cis*-Pt.

* compound (**2**) precipitated at a concentration of 1 mM in the cell culture (the results were discarded)

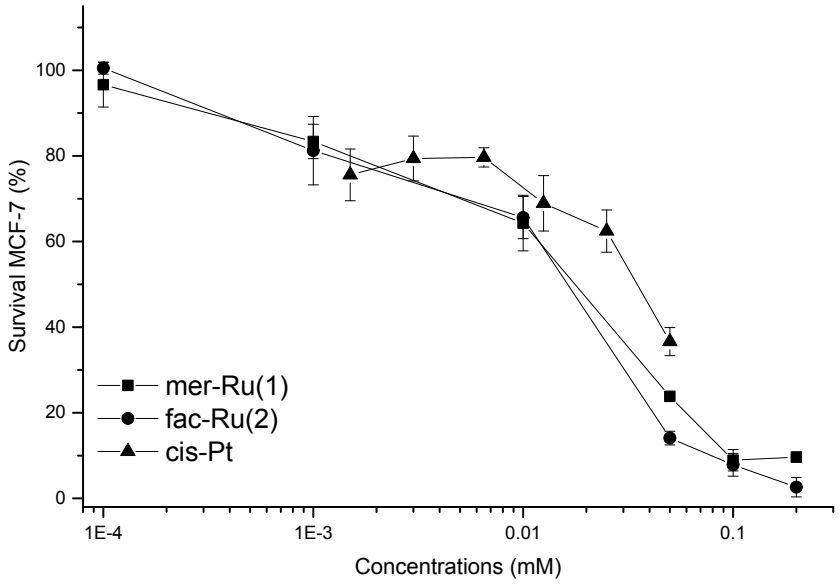

Figure S9. The survival rate of MCF-7 cells after 48 hours of incubation with compound (**1**), (**2**), and *cis*-Pt.

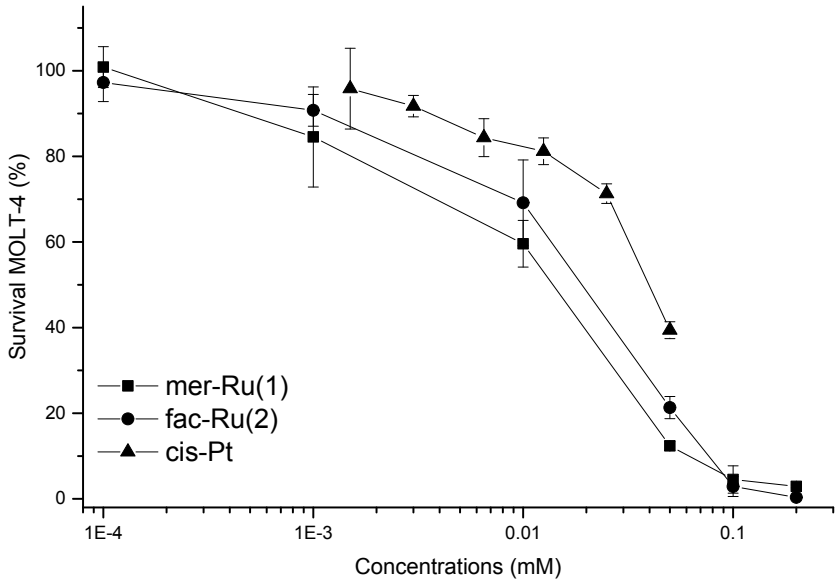

Figure S10. The survival rate of MOLT-4 cells after 48 hours of incubation with compound (**1**), (**2**), and *cis*-Pt.

Digestion of plasmid DNA with BamHI restriction nuclease

0.5 μg of plasmid DNA (pcDNAHisC with insert, total length 8.2 kbp) containing a unique *BamHI* restriction site was dissolved in a 1x *BamHI* reaction buffer and incubated overnight at 37 °C with the test compounds**,** daunorubicin or *cis*-Pt. Daunorubicin and *cis*-Pt were used as reference compounds. The final concentration of the ruthenium(III) compounds, daunorubicin and *cis*-Pt in samples was 10 or 100 μM. In the next step, the reaction mixtures were digested with *BamHI* restriction endonuclease (2U/μL) for 3h at 37 °C. The total reaction volume was 10μL. The products of the reaction were subjected to the 1% agarose gel electrophoresis in TBE buffer. The gel was stained with ethidium bromide and DNA fragments were visualised under a UV lamp (GBox, Syngene).

Result of the digestion of plasmid DNA with BamHI restriction nuclease

8.2 kbp plasmid DNA (pcDNA3.1HisC) containing a single *BamHI* cleavage site was incubated with test compounds or daunorubicin. Next, the plasmid DNA was digested with *BamH1* restriction endonuclease. Upon digestion, plasmid DNA is converted into a linear

form, while the undigested plasmid exists in circular and superhelical forms. All these forms differ in electrophoretic mobility and can be separated and analysed by standard agarose gel electrophoresis. Intercalating agents inhibit the enzymatic conversion of the circular form of plasmid DNA into a linear form, which can be easily detected and confirmed by electrophoretic analysis. As shown on **Figure S9**, non-digested pcDNA3.1HisC (with cDNA insert, total length 8.2kbp) exists predominantly in superhelical and circular forms (lane 1). Upon action of *BamHI*, the plasmid DNA is completely converted to a linear form, which migrates in an agarose gel as a single 8.2 kbp band (lane 2). In the presence of daunorubicin (a strong intercalating agent) and *cis*-Pt (which forms mainly intrastrand crosslink DNA adducts), the conversion of circular DNA into linear form catalysed by *BamHI* is significantly inhibited (lane 3, 4 and 11, respectively). Interestingly, in the presence of compounds (**1**), (**2**) and **dmpbt** both the circular and linear form of plasmid DNA can be detected (lanes 5, 7 and 9 respectively). The presence of a circular form of DNA suggests that (**1**), (**2**) and **dmpbt** may interact with plasmid DNA and inhibit the *BamHI*-driven conversion of circular DNA into linear counterpart. The inhibitory effects of test compounds on the digestion of circular DNA with *BamHI* were similar to *cis*-Pt and daunorubicin used at the concentration of 10 μM. However, when compared to *cis*-Pt and daunorubicin at the concentration of 100 μM, the test compounds (**1**), (**2**) and **dmpbt** seem to be very weaker DNA-binding agents.

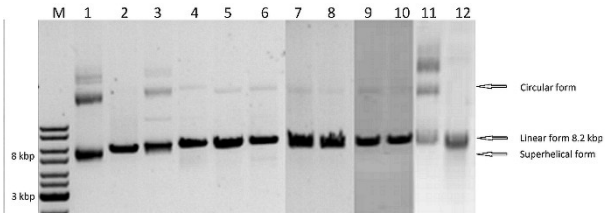

Figure S11. The influence of test compounds, *cis*-Pt and daunorubicin on digestion of plasmid DNA with endonuclease *BamH1*. M – DNA marker; lane 1 – non-digested plasmid DNA; lane 2 – plasmid DNA treated with *BamH1* (linearized plasmid DNA); 3 – plasmid DNA + Daunorubicin (100 μM); lane 4 – plasmid DNA + Daunorubicin (10 μM); lane 5 - plasmid DNA + (**1**) (100 μM); lane 6 – plasmid DNA + (**1**) (10 μM); lane 7 – plasmid DNA + (**2**) (100 μM); lane 8 – plasmid DNA + (**2**) (10 μM); lane 9 – plasmid DNA + (dmpbt) (100 μM); lane 10 – plasmid DNA + (dmpbt) (10 μM); lane 11 – plasmid DNA+ *cis*-Pt (100 μM); lane 12 – plasmid DNA + *cis*-Pt (10 μM). Samples in lanes 3-12 were digested with *BamH1*.

Interaction of (1), (2), dmpbt, and *cis*-Pt with DNA – circular dichroism (CD)

Studied samples contained bovine thymus DNA (0.2 mg/ml) dissolved in phosphate buffered saline (PBS). The DMSO solutions of test compounds were used at the concentration of 50 μM, yielding 0.5% final DMSO concentration in the sample. The CD spectra were recorded after 15 min of incubation with the DNA using Jasco J-815 dichrograph. The measurements were performed over a 200-320 nm range at 23°C, using a quartz cell with an optical path length of 1 cm. The CD spectra of DNA incubated with the test compounds were compared with the reference spectrum recorded for a sample containing 0.2 mg/ml for bovine thymus DNA in the presence of 0.5% DMSO. Daunorubicin a potent DNA intercalator was used in a positive control experiment.

Result of the Interaction of (1), (2), dmpbt, and *cis*-Pt with DNA – circular dichroism (CD)

The effect of ruthenium(III) compounds on the conformation of the DNA was measured by circular dichroism. Daunorubicin (a strong intercalating agent) and *cis*-Pt (crosslinks N7 of DNA purine bases) were used as reference compounds.[102] Comparison of CD spectra

(**Figure S10**) confirms that daunorubicin induces a conformational change in DNA. However, in the presence of the test compounds (**1**), (**2**) and dmpbt no significant changes in DNA spectra were detected. This suggests that test compounds have rather weak impact on the secondary structure of DNA but does not rule out the possibility of binding to DNA.

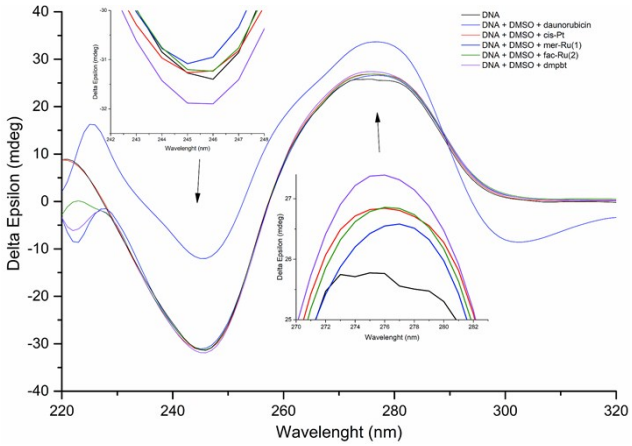

Figure S12. CD spectra of calf thymus DNA recorded in the presence of compounds (**1**), dmpbt, (**2**), *cis*-Pt and daunorubicin. Spectra were recorded at room temperature, 15 min. after addition of test compounds (50 μM). DNA + 0.5% DMSO served as a control.

The results of DNA plasmid digestion demonstrate that ruthenium complexes interact with DNA but the character of these interactions requires further detailed research. Circular dichroism data suggest that ruthenium complexes do not intercalate to DNA. However, other modes of DNA binding can not be excluded. For example, ruthenium complexes may act as monodentate DNA ligands. As reported previously, monodentate DNA ligands do not cause substantial changes in DNA spectra[3].

The results of the research DNA interactions with *mer*- and *fac*- ruthenium(III) complexes, showed that DNA is not the primary target for our complexes. **It is also possible that our complexes target different protein(s) depending on the cell line** because cell lines differ significantly in the expression of proteins.

[1]Virupaxappa, H., V.K. Revankar, and V.B. Mahale, *Synthesis, characterization and biological studies of 2-(3,5-dimethyl-pyrazol-1-yl)benzothiazole complexes of cobalt(II), nickel(II) and copper(II).* Transition Metal Chemistry, 1993. **18**(2): p. 158-162.

[2]Edwards, D.A. and R. Richards, *Low-frequency vibrational-spectra of some triphenylophosphine complexes of copper(I) and silver(I).* Spectrochimica Acta Part a-Molecular and Biomolecular Spectroscopy, 1978. **34**(2): p. 167-171.

[3] Macquet, J.P. and J.L. Butour, *Circular-dichroism study of DNA platinum complexes-differentation between monofunctional, cis-bidentate and trans-bidentate platinum fixation on a series of DNAs.* European Journal of Biochemistry, 1978. **83**(2): p. 375-387.